Dynamic Analysis of a One-Dimensional Poroviscoelastic Column

M. Schanz
Institute of Applied Mechanics,
Technical University Braunschweig,
D-38023 Braunschweig, Germany

A. H.-D. Cheng
Department of Civil and
Environmental Engineering,
University of Delaware,
Newark, DE 19716

The response due to a dynamic loading of a poroviscoelastic one-dimensional column is treated analytically. Biot's theory of poroelasticity is generalized to poroviscoelasticity using the elastic-viscoelastic correspondence principle in the Laplace domain. Damping effects of the solid skeletal structure and the solid material itself are taken into account. The fluid is modeled as in the original Biot's theory without any viscoelastic effects. The solution of the governing set of two coupled differential equations known from the purely poroelastic case is converted to the poroviscoelastic solution using the developed elastic-viscoelastic correspondence in Laplace domain. The time-dependent response of the column is achieved by the ''Convolution Quadrature Method'' proposed by Lubich. Some interesting effects of viscoelasticity on the response of the column caused by a stress, pressure, and displacement loading are studied. [DOI: 10.1115/1.1349416]

1 Introduction

For a wide range of fluid infiltrated materials, such as water saturated soils, oil impregnated rocks, or air filled foams, the elastic theory is a crude approximation. Due to presence of a second, interacting continuum, a different theory is necessary. The theory of porous materials containing a viscous fluid, known as the theory of poroelasticity, was introduced by Biot [1]. In subsequent years, this theory was extended to the anisotropic case ([2]), and also to dynamics ([3]). Following this development, the dynamic as well as the quasi-static analysis of a fully saturated porous continuum is possible. A comprehensive review of the quasi-static theory in rock mechanics can be found in the work of Detournay and Cheng [4].

In addition to the effect of the viscous fluid diffusion in the pores, the solid constituent, its skeleton, and its interaction with partially entrapped fluid can introduce time-dependent behavior as viscoelastic material. Further on, the rheology of pore fluid can exhibit viscoelastic behavior as well. This effect, however, will not be taken into account in the study here. The implementation of the solid viscoelastic effects in the theory of poroelasticity was first introduced by Biot [5]. Further work on this topic was done in the quasi-static case in [6] and in dynamics in [7], to cite a few. The last cited paper generalized Biot's theory to partially saturated continua.

Recently, a representation of the poroviscoelastic theory based on rheological modeling at micromechanical level was published by Abousleiman et al. [8]. It was argued that to have a physically consistent model, the rheology for the solid constituent and the skeletal structure should be clearly separated, and then combined to form a bulk continuum model. Based on this model, originally in quasi-static range, the current work examines its dynamic responses. The set of the governing differential equations for the dynamic case are deduced for a one-dimensional column. The corresponding analytical solution for one-dimensional column for the poroelastodynamic case has been presented by Schanz and Cheng [9]. The extension to poroviscoelasticity of this solution will be done in Laplace domain with the help of the elastic-viscoelastic correspondence principle.

With this solution, the frequency-dependent response of this column due to an impulsive load can be studied with respect to the influence of the viscoelasticity by taking the real part of the complex Laplace variable to zero. Then, the response of an arbitrary dynamical loaded system in time domain is given by the convolution integral of the impulse response function and the time-dependent loading. This convolution integral is numerically evaluated by the so-called ''Convolution Quadrature Method'' proposed by Lubich [10]. The weights of this quadrature formula are determined from the Laplace transformed impulse response function and a linear multistep method. In this method, no solution in time domain of the original problem is necessary. Through a series of stringent tests that includes a comparison with the highly acclaimed Dubner-Abate-Durbin-Crump method (e.g., [11] or [12]), our experience indicates that the Lubich method is one of the most robust in performing the inversion of wave-like functions that involves a significant number of cycles resulting from impact loading. This method has been, among other applications, successfully applied to a time domain formulation of the boundary element method ([13]).

2 Governing Equations

Following Biot's approach to model the behavior of porous media, the constitutive equations can be expressed as ([1])

$$\sigma_{ij} = 2G\epsilon_{ij} + \left(K - \frac{2}{3}G\right)\epsilon_{kk}\delta_{ij} - \alpha\delta_{ij}p \tag{1a}$$

$$\zeta = \alpha\epsilon_{kk} + \frac{\phi^2}{R}p, \tag{1b}$$

in which σ_{ij} denotes the total stress, p the pore pressure, ϵ_{ij} the strain of the solid frame, ζ the variation of fluid volume per unit reference volume, and δ_{ij} the Kronecker delta. In the above, the sign conventions for stress and strain follow that of elasticity, namely, tensile stresses and strains are denoted positive. The Latin indices takes the values 1, 2, 3 or 1, 2 in three-dimensional or two-dimensional cases, respectively, where summation convention is implied over repeated indices. The bulk material is defined by the material constants shear modulus G and the drained bulk compression modulus K. Biot's effective stress coefficient α, the porosity ϕ, and R complete the set of material parameters.

Contributed by the Applied Mechanics Division of THE AMERICAN SOCIETY OF MECHANICAL ENGINEERS for publication in the ASME JOURNAL OF APPLIED MECHANICS. Manuscript received by the ASME Applied Mechanics Division, December 12, 1999; final revision, July, 2000. Associate Editor: D. A. Siginer. Discussion on the paper should be addressed to the Editor, Professor Lewis T. Wheeler, Department of Mechanical Engineering, University of Houston, Houston, TX 77204-4792, and will be accepted until four months after final publication of the paper itself in the ASME JOURNAL OF APPLIED MECHANICS.

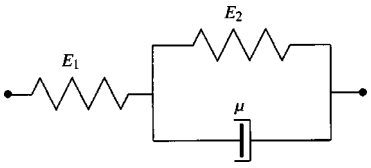

Fig. 1 One-dimensional rheological three-parameter model

In the constitutive equations above the only damping effects taken into account are caused by the interaction of the viscous fluid and the elastic solid. Introducing additionally viscoelasticity is done by means of the elastic-viscoelastic correspondence principle, as shown by Biot [5]. In a typical implementation in Laplace domain, the material constants shown in (1) are replaced by the corresponding functions of the Laplace variable, i.e., they become time-dependent. However, this approach provides little physical insight into the rheological models introduced, because the effective stress coefficient α, or R, or the pair of coefficients Q and R in the partial stress formulation of Biot [5], have no simple relation to the compression or shear behavior of the constituents. Rather, considerations of constitutive relation at micromechanical level ([4]) lead to a more rational model for our purpose

$$\alpha = 1 - \frac{K}{K_s} \tag{2}$$

and

$$R = \frac{\phi^2 K_f K_s^2}{K_f(K_s - K) + \phi K_s(K_s - K_f)}, \tag{3}$$

where K_s denotes the compression modulus of the solid grains and K_f the compression modulus of the fluid. With these expressions we are able to discuss how to implement viscoelastic behavior from a physical point of view.

Next, viscoelastic constitutive equations are introduced. From the two most common representations of viscoelastic constitutive equations, the hereditary integral or the differential operator formulation ([14]), the differential operator formulation is suitable to our purpose. The simplest model ensuring causal behavior is the three-parameter model, sometimes referred to as Kelvin-Voigt model (see Fig. 1). When the system is subjected to a step load, it instantly deforms in an elastic state characterized by the spring constant E_1. As time progresses, the resistance offered by the dash-pot diminishes and the system softens. At large times, the apparent spring constant becomes $E = E_1 E_2/(E_1 + E_2)$, which is smaller than the initial modulus E_1. The speed of the creep is regulated by the dash-pot viscosity μ. A characteristic time scale for the creep can be defined as $q = \mu/E_2$. The appropriate constitutive relation is given as

$$\begin{gathered} p = \frac{\mu}{E_1 + E_2}, \quad E = \frac{E_1 E_2}{E_1 + E_2}, \quad q = \frac{\mu}{E_2} \\ p\frac{\mathrm{d}}{\mathrm{d}t}\sigma + \sigma = E\left(\varepsilon + q\frac{\mathrm{d}}{\mathrm{d}t}\varepsilon\right). \end{gathered} \tag{4}$$

To find the elastic-viscoelastic correspondence, the differential Eq. (4) is transformed to Laplace domain

$$\hat{\sigma}(ps + 1) = E\hat{\epsilon}(1 + qs), \tag{5}$$

with $\mathcal{L}\{f(t)\} = \hat{f}(s)$ denotes the Laplace transform, with the complex Laplace variable s. Compared with Hook's law the elastic-viscoelastic correspondence is clearly observed,

$$E \to E\frac{1 + qs}{1 + ps}, \tag{6}$$

where the right-hand side is often called complex modulus.

In the explicit form of (2) and (3), the Kelvin-Voigt model can be applied to each of the moduli, corresponding to different physical effects. In detail:

- Replacing G by the complex modulus $\hat{G}(s)$ models a viscoelastic shear behavior of the solid frame.
- Replacing K_s by the complex modulus $\hat{K}_s(s)$ models a viscoelastic behavior of solid grains against volumetric deformation. This is necessary if the material has its own damping mechanism.
- Replacing K by the complex modulus $\hat{K}(s)$ models a viscoelastic behavior of the solid skeleton against volumetric deformation. Such a behavior can be caused, e.g., by micropores which are not connected to the main part of the fluid. The fluid in micropores can propagate through microcracks in the material causing damping due to the time required to reach localized equilibrium.
- Replacing K_f by the complex modulus $\hat{K}_f(s)$ models a viscoelastic behavior of the fluid. This, however, will not be attempted here for the following reasons: First, most pore fluids such as water or air are not viscoelastic. Second, a viscoelastic fluid can have shear stresses, which will interact with the surrounding solid. These effects are not modeled in Biot's theory. An arbitrarily generalization will not lead to a consistent theory.

Summarizing, in the following, a time-dependent compression and shear modulus of the solid $\hat{K}_s(s)$ and $\hat{G}(s)$ and a time-dependent bulk modulus $\hat{K}(s)$ are taken into account. This leads to the poroviscoelastic constitutive equations in Laplace domain as

$$\hat{\sigma}_{ij} = 2\hat{G}\hat{\epsilon}_{ij} + \left(\hat{K} - \frac{2}{3}\hat{G}\right)\hat{\epsilon}_{kk}\delta_{ij} - \hat{\alpha}\,\delta_{ij}\hat{p} \tag{7a}$$

$$\hat{\zeta} = \hat{\alpha}\hat{\epsilon}_{kk} + \frac{\phi^2}{\hat{R}}\hat{p}, \tag{7b}$$

with

$$\hat{\alpha}(s) = 1 - \frac{\hat{K}(s)}{\hat{K}_s(s)}$$

and

$$\hat{R}(s) = \frac{\phi^2 K_f \hat{K}_s^2(s)}{K_f(\hat{K}_s(s) - \hat{K}(s)) + \phi\hat{K}_s(s)(\hat{K}_s(s) - K_f)}. \tag{8}$$

Note, every formerly constant which is now indicated with $\hat{(\ )}$ is a function of s, respectively, of time. In the following, it is assumed that $\hat{K}_s(s)$, $\hat{G}(s)$, and $\hat{K}(s)$ are modeled as a three parameter model using the correspondence relation (6)

$$\hat{K}(s) = K\frac{1 + q_k s}{1 + p_k s}, \quad \hat{K}_s(s) = K_s\frac{1 + q_{ks} s}{1 + p_{ks} s}, \quad \hat{G}(s) = G\frac{1 + q_g s}{1 + p_g s}. \tag{9}$$

This completes the constitutive equations for a poroviscoelastic model. In the following, the functional argument (s) will be dropped for brevity.

Now, the governing set of differential equations are achieved by inserting (7) in the Laplace transformed dynamic equilibrium

$$\hat{\sigma}_{ij,j} + \hat{F}_i = \rho s^2 \hat{u}_i + \phi\rho_f s^2 \hat{v}_i, \tag{10}$$

and in the continuity equation

$$s\hat{\zeta} + \hat{q}_{i,i} = 0, \tag{11}$$

where $\rho = \rho_s(1 - \phi) + \phi\rho_f$ is the bulk density, with ρ_s and ρ_f denoting the solid and fluid density, respectively. As well the displacements of the solid are denoted by $\hat{u}_i$ and the relative fluid to solid displacements by $\hat{v}_i$. In Eqs. (10) and (11) and in the

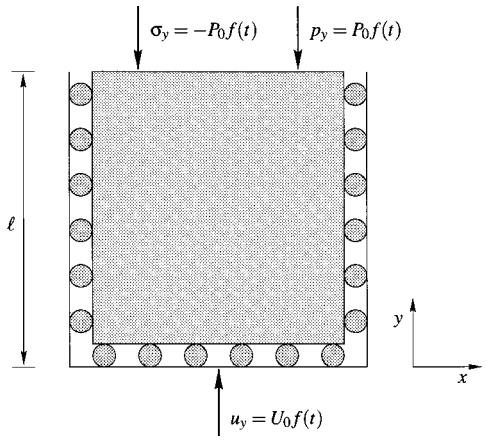

Fig. 2 One-dimensional column under dynamic loading

following, vanishing initial conditions for all variables are assumed. $\hat{F}_i$ are the bulk body forces which are neglected in the following, as only perturbation from the hydrostatic state is sought, and $\hat{q}_i = \phi s \hat{v}_i$ denotes the specific flux of the fluid. Finally, the derivative with respect to the spatial variable x_i is abbreviated by $(\,)_{,i}$.

Proceeding in taking Darcy's law

$$\hat{q}_i = -\kappa\left(\hat{p}_{,i} + s^2\rho_f\hat{u}_i + \frac{\rho_a + \phi\rho_f}{\phi}s^2\hat{v}_i\right) \tag{12}$$

into account, where κ denotes the permeability and ρ_a the apparent mass density, the final set of differential equations for the displacements $\hat{u}_i$ and the pore pressure $\hat{p}$ are achieved,

$$\hat{G}\hat{u}_{i,jj} + \left[\hat{K} + \frac{1}{3}\hat{G}\right]\hat{u}_{j,ij} - (\hat{\alpha} - \beta)\hat{p}_{,i} - s^2(\rho - \beta\rho_f)\hat{u}_i = 0 \tag{13}$$

$$\frac{\beta}{s\rho_f}\hat{p}_{,ii} - \frac{\phi^2 s}{\hat{R}}\hat{p} - (\hat{\alpha} - \beta)s\hat{u}_{i,i} = 0, \tag{14}$$

with the abbreviation

$$\beta = \frac{\phi^2 s\kappa\rho_f}{\phi^2 + s\kappa(\rho_a + \phi\rho_f)}. \tag{15}$$

For simplicity, the apparent mass density ρ_a is assumed to be frequency independent as $\rho_a \approx 0.66\phi\rho_f$ ([15]). With this set of equations the dynamic behavior of a poroviscoelastic continuum is completely defined.

3 Analytical Solution in One Dimension

A one-dimensional column of length l as sketched in Fig. 2 is considered. It is assumed that the sidewalls and the bottom are rigid, frictionless, and impermeable. Hence, the displacements normal to the surface are blocked and the column is otherwise free to slide parallel to the wall. At the top, the stress σ_y and the pressure p are prescribed. Due to these restrictions only the displacement u_y and the pore pressure p remain as degrees-of-freedom. This one-dimensional example can be used to study the influence of poroelastic parameters on wave propagation, or it can be used for actual application of finite and also semi-infinite columns by setting the layer depth l large. Here, we are particular interested in observing the interplay of the two compressional waves, a fast and a slow wave.

The governing set of differential Eqs. (13) and (14) is reduced to two scalar, coupled ordinary differential equations

$$\hat{E}\hat{u}_{y,yy} - (\hat{\alpha} - \beta)\hat{p}_{,y} - s^2(\rho - \beta\rho_f)\hat{u}_y = 0 \tag{16}$$

$$\frac{\beta}{s\rho_f}\hat{p}_{,yy} - \frac{\phi^2 s}{\hat{R}}\hat{p} - (\hat{\alpha} - \beta)s\hat{u}_{y,y} = 0, \tag{17}$$

with the modulus $\hat{E} = \hat{K} + (4/3)\hat{G}$. The boundary conditions are

$$\hat{u}_y(y=0) = U_0, \quad \hat{q}(y=0) = 0$$

and

$$\hat{\sigma}(y=l) = -P_0, \quad \hat{p}(y=l) = P_0, \tag{18}$$

where an impulse function for the temporal behavior $f(t) = \delta(t)$, with $\delta(t)$ denoting the Dirac distribution, is assumed, together with vanishing initial conditions. Each of the nonzero boundary conditions in (18) represents a different type of loading. Due to the neglected body forces, this is a system of homogeneous ordinary differential equations with inhomogeneous boundary conditions. Such a system has been solved for the nonviscoelastic case in [9]. Inserting in these solutions the elastic-viscoelastic correspondences (9) leads to the solution of the poroviscoelastic problem above. As we are dealing with a linear problem the superposition principle is valid. Therefore, the solution can be divided in the three different load cases:

Stress Boundary Conditions. $\hat{u}_y(y=0) = 0$, $\hat{\sigma}(y=l) = -P_0$ and $\hat{p}(y=l) = 0$

$$\hat{u} = \frac{P_0}{\hat{E}(d_1\lambda_3 - d_3\lambda_1)}\left[\frac{d_3(e^{-\lambda_1(l-y)} - e^{-\lambda_1(l+y)})}{1 + e^{-2\lambda_1 l}} - \frac{d_1(e^{-\lambda_3(l-y)} - e^{-\lambda_3(l+y)})}{1 + e^{-2\lambda_3 l}}\right] \tag{19}$$

$$\hat{p} = \frac{P_0 d_1 d_3}{\hat{E}(d_1\lambda_3 - d_3\lambda_1)}\left[\frac{d_3(e^{-\lambda_1(l-y)} + e^{-\lambda_1(l+y)})}{1 + e^{-2\lambda_1 l}} - \frac{d_1(e^{-\lambda_3(l-y)} + e^{-\lambda_3(l+y)})}{1 + e^{-2\lambda_3 l}}\right] \tag{20}$$

Pressure Boundary Conditions. $\hat{u}_y(y=0) = 0$, $\hat{\sigma}(y=l) = 0$ and $\hat{p}(y=l) = P_0$

$$\hat{u} = \frac{P_0}{\hat{E}(d_1\lambda_3 - d_3\lambda_1)}\left[\frac{(\hat{E}\lambda_3 - \hat{\alpha}d_3)(e^{-\lambda_1(l-y)} - e^{-\lambda_1(l+y)})}{1 + e^{-2\lambda_1 l}} - \frac{(\hat{E}\lambda_1 - \hat{\alpha}d_1)(e^{-\lambda_3(l-y)} - e^{-\lambda_3(l+y)})}{1 + e^{-2\lambda_3 l}}\right] \tag{21}$$

$$\hat{p} = \frac{P_0}{\hat{E}(d_1\lambda_3 - d_3\lambda_1)}\left[\frac{d_1(\hat{E}\lambda_3 - \hat{\alpha}d_3)(e^{-\lambda_1(l-y)} + e^{-\lambda_1(l+y)})}{1 + e^{-2\lambda_1 l}} - \frac{d_3(\hat{E}\lambda_1 - \hat{\alpha}d_1)(e^{-\lambda_3(l-y)}e^{-\lambda_3(l+y)})}{1 + e^{-2\lambda_3 l}}\right] \tag{22}$$

Displacement Boundary Conditions. $\hat{u}_y(y=0) = U_0$, $\hat{\sigma}(y=l) = 0$ and $\hat{p}(y=l) = 0$

$$\hat{u} = \frac{U_0}{\hat{E}(\lambda_3^2 - \lambda_1^2)}\left[\frac{(\hat{E}\lambda_3^2 + s^2(\hat{\alpha}\rho_f - \rho))(e^{-\lambda_1(2l-y)} + e^{-\lambda_1 y})}{1 + e^{-2\lambda_1 l}} - \frac{(\hat{E}\lambda_3^2 + s^2(\hat{\alpha}\rho_f - \rho))(e^{-\lambda_3(2l-y)} + e^{-\lambda_3 y})}{1 + e^{-2\lambda_3 l}}\right] \tag{23}$$

Table 1 Material data of Berea sandstone, a soil, and a sediment

	$K\left[\frac{N}{m^2}\right]$	$G\left[\frac{N}{m^2}\right]$	$\rho\left[\frac{kg}{m^3}\right]$	φ	$K_s\left[\frac{N}{m^2}\right]$	$\rho_f\left[\frac{kg}{m^3}\right]$	$K_f\left[\frac{N}{m^2}\right]$	$\kappa\left[\frac{m^4}{Ns}\right]$
rock	8×10^9	6×10^9	2458	0.19	3.6×10^{10}	1000	3.3×10^9	1.9×10^{-10}
soil	2.1×10^8	9.8×10^7	1884	0.48	1.1×10^{10}	1000	3.3×10^9	3.55×10^{-9}
sediment	3.7×10^7	2.2×10^7	1396	0.76	3.6×10^{10}	1000	2.3×10^9	1×10^{-8}

$$\hat{p}=\frac{U_0}{\hat{E}(\lambda_3^2-\lambda_1^2)}\left[\frac{d_1(\hat{E}\lambda_3^2+s^2(\hat{\alpha}\rho_f-\rho))(e^{-\lambda_1(2l-y)}-e^{-\lambda_1 y})}{1+e^{-2\lambda_1 l}}\right.$$
$$\left.-\frac{d_3(\hat{E}\lambda_3^2+s^2(\hat{\alpha}\rho_f-\rho))(e^{-\lambda_3(2l-y)}-e^{-\lambda_3 y})}{1+e^{-2\lambda_3 l}}\right] \quad (24)$$

The corresponding stresses and fluxes are calculated with the one-dimensional form of the constitutive Eq. (7*a*)

$$\hat{\sigma}(s,y)=\hat{E}\hat{u}_{y,y}-\hat{\alpha}\hat{p} \quad (25)$$

and the one-dimensional form of Darcy's law (12)

$$\hat{q}(s,y)=-\frac{\beta}{s\rho_f}(\hat{p}_{,y}+s^2\rho_f\hat{u}_y). \quad (26)$$

With the solutions above, the frequency-dependent harmonic response of a one-dimensional poroviscoelastic column can be studied by taking $s=-i\omega$. However, the time-dependent response due to an arbitrary excitation $f(t)$, is achieved by the convolution integral, e.g., for the displacements

$$u_y(t,y)=\int_0^t \mathcal{L}^{-1}\{\hat{u}_y(s,y)\}(\tau,y)f(t-\tau)d\tau, \quad (27)$$

where $\mathcal{L}^{-1}$ is the inverse Laplace transform operator. Another way to obtain solution of arbitrary transient input is to take the advantage of the property of Laplace transform

$$u_y(t,y)=\mathcal{L}^{-1}\{\hat{u}_y(s,y)\hat{f}(s)\} \quad (28)$$

where $\hat{f}(s)$ is the Laplace transform of the boundary condition $f(t)$.

We now have two possibilities to evaluate the response in time domain. We can either multiply the impulse response functions (19)–(24) by the input excitation in Laplace domain, $\hat{f}(s)$, with a subsequent numerical inverse transformation as indicated in (28), or we use the ''Convolution Quadrature Method'' proposed by Lubich [10] to directly tackle (27). The first choice, with all its advantages and disadvantages, is the traditional approach (see, e.g., [12] or [11]). But, in this case here, where the one function in the convolution integral (27) is available in Laplace domain and the other function in time domain, it is preferable to take the Convolution Quadrature Method. This method approximates the convolution integral (27) numerically by a quadrature formula

$$u_y(n\Delta t)=\sum_{k=0}^{n}\omega_{n-k}(\Delta t)f(k\Delta t), \quad n=0,1,\ldots,N, \quad (29)$$

whose weights $\omega_{n-k}(\Delta t)$ are determined with the help of the Laplace transformed impulse response functions $\hat{u}_y(s,y)$ and a function $\gamma(s)$ that defines the linear multistep method

$$\omega_n(\Delta t)-\frac{\mathcal{R}^{-n}}{L}\sum_{l=0}^{L-1}\hat{u}_y\left(\frac{\gamma(\mathcal{R}e^{il2\pi/L})}{\Delta t}\right)e^{-inl2\pi/L}. \quad (30)$$

More details of the method and the definition of parameters can be found in Appendix A. In the following, this method is used to perform the time-dependent responses, choosing a backward differentiation formula of order 2 (BDF 2) as the underlying multistep method.

4 Results in Frequency and Time Domain

With the analytical solution developed in Section 3, the influence of different damping mechanisms is studied. Three very different materials, ranked in descending order of stiffness, a rock (Berea sandstone) ([16]), a soil (coarse sand) ([17]), and a seabed sediment ([18]), are chosen to cover a wide range of material properties. The material data are given in Table 1. We observe that the stiffness of the material, in terms of frame bulk modulus and shear modulus, spans more than two orders of magnitude. The value of bulk density decreases as porosity increases. The fluid bulk modulus for sediment is different because sea water was referred in [18]. The bulk moduli of solid grain are about the same. We should point out that for the soil case, dense sand saturated with silicon oil was used in [17]. In Table 1, however, the fluid was changed to water with other material coefficients consistently converted. Finally, we observe that the permeability also spans more than two orders of magnitude.

In the constitutive Eq. (7) the bulk modulus $\hat{K}$, the shear modulus $\hat{G}$, and the compression modulus of the solid itself $\hat{K}_s$ are each chosen to be viscoelastic, modeled by a three-parameter model. For each of them, the values of p and q need to be given. However, to the authors' best knowledge, no such data have been reported in the literature. Therefore, the same set of data is somewhat arbitrarily chosen for the three materials. To compare the influence of viscoelasticity in different moduli on the dynamic response, four different cases are considered:

Case 1: Only the bulk compression modulus $\hat{K}(s)$ is modeled viscoelastic: $p_k=1[\frac{1}{s}]$, $q_k=1.5[\frac{1}{s}]$ and $p_{ks}=p_g=q_{ks}=q_g=0[\frac{1}{s}]$.

Case 2: Only the shear modulus $\hat{G}(s)$ is modeled viscoelastic: $p_g=1[\frac{1}{s}]$, $q_g=1.5[\frac{1}{s}]$ and $p_{ks}=p_k=q_{ks}=q_k=0[\frac{1}{s}]$.

Case 3: Only the compression modulus of the solid material $\hat{K}_s(s)$ is modeled viscoelastic: $p_{ks}=1[\frac{1}{s}]$, $q_{ks}=1.5[\frac{1}{s}]$ and $p_k=p_g=q_k=q_g=0[\frac{1}{s}]$.

Case 4: The purely poroelastic case without any viscoelasticity: $p_{ks}=q_{ks}=p_k=p_g=q_k=q_g=0[\frac{1}{s}]$.

Before solving the transient problems, the frequency response of a column with length $l=1$ m is first considered. In Fig. 3 the absolute value of the displacements $\hat{u}_y(\omega,y=l)$ at the top of the column are plotted versus frequency ω for the three materials. As boundary condition, a constant step pressure loading (without total stress) is assumed. In Fig. 3 we observe resonance peaks as expected. The first resonance frequency is around 2000 Hz for the sediment, which increases to about 5000 Hz for the rock. The various curves correspond to different assumptions of viscoelasticity, referred to as case 1 to 4 in the above. It is found that the sediment response is least affected by viscoelastic effect—there is basically no shift in eigenfrequencies and only a slight damping in response amplitude. This is in accordance with our model, be-

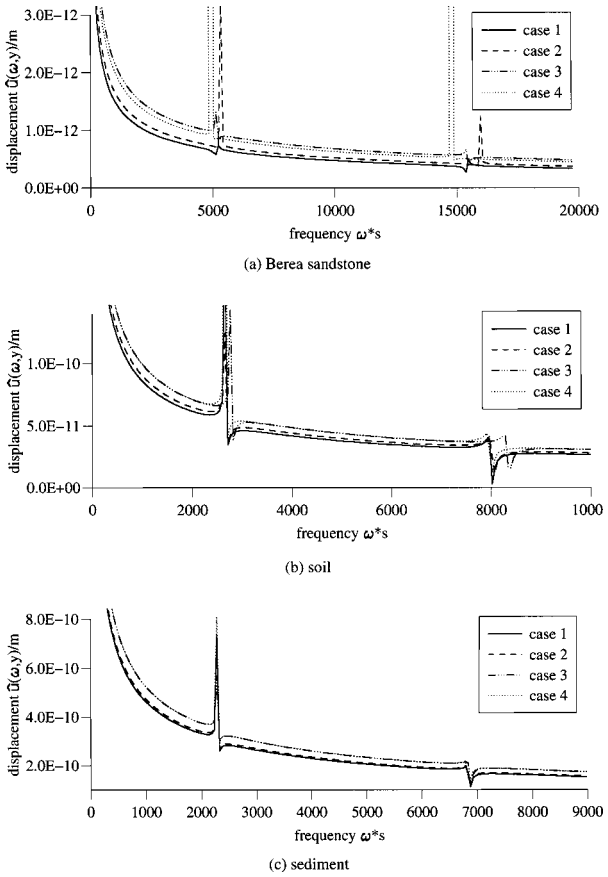

Fig. 3 Absolute value of the displacements $|\hat{u}_y(\omega, y=l)|$ at the top of the column versus frequency ω

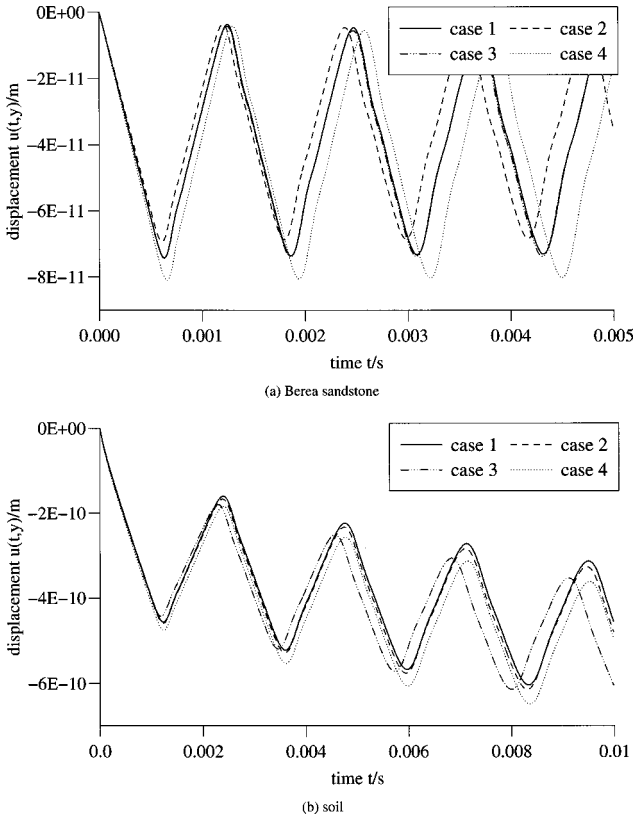

Fig. 4 Displacements u_y $(t, y=l)$ at the top of the column versus time t

cause the sediment bulk property is dominated by the fluid, which is elastic. The viscoelastic solid hence contributes to only a secondary influence. The soil response is also less influenced. There is a small shifting of eigenfrequencies, and a somewhat larger damping than the sediment case. The largest effects are found in the rock material. Not only there exists larger damping, particularly on the resonance peaks, but also significant shift of eigenfrequencies occurs. We further observe that for all materials, the largest damping results from the viscoelasticity of bulk compression modulus. For soil, the largest shift of eigenfrequencies results from the viscoelastic effect of $\hat{K}_s$, compared to rock where $\hat{G}$ has the most influence. This shows that the effect of each modulus is different in different materials.

For the frequency response of the other two boundary conditions, a stress and a displacement loading, the influence of viscoelasticity exhibits similar trend. Hence it is enough to show the results for just this boundary condition.

Now, the time-dependent behavior is considered. Due to the relative insensitivity of sediment response to viscoelasticity, only results for the two other materials are presented. In Fig. 4 the displacements $u(t, y=l)$ at the top of the column, caused by a step stress loading $\sigma(t, y=l) = -H(t) N/\mathrm{m}^2$, are depicted versus time. In each of the curves, a different time-step size is used for the Lubich method, due to different wave speeds of the materials. For the Berea sandstone $\Delta t = 1 \times 10^{-5}$ s and for the soil $\Delta t = 2 \times 10^{-5}$ s are used, with $N = 500$ time steps. As with any numerical method, too large a time-step size leads to worse results due to inadequate approximation of the time history of the displacements.

In Fig. 4, the rock displacements show an oscillation similar to that for an elastic material, whereas for the soil, the oscillation is combined with a settlement, due to the well-known consolidation effect. We notice that the wave speed is modified in both materials. Case 4, the case without viscoelasticity, has the slowest wave speed, by observing the time it takes the wave to transverse the column. This is not surprising, because by setting the two parameters p and q in (6) to zero, case 4 has the smallest modulus. In the viscoelastic cases, the apparent modulus of the material is between $1.5E$ for small time (or high frequency), and E for large time (or low frequency), due to the p and q values used. Hence the wave speed of the viscoelastic and the elastic cases should not be directly compared. However, among the viscoelastic cases, we can compare and observe that different modulus has different effect on the two materials. The fastest wave in the rock is associated with the viscoelasticity of shear modulus. The fastest wave in soil, on the other hand, is observed to be associated with the solid compression modulus. The oscillation amplitude is found to be the smallest also in these two cases, respectively, for soil and rock. These are consistent with the observation in frequency domain.

We further tested cases with an increased damping value p, which is observed to enhance the damping effect. But as mentioned before, no measured damping values are available. It is not possible to say whether these assumed damping values are realistic or not. Therefore, these results are not presented here.

We next investigate wave propagation in this one-dimensional column with the aim of capturing the two compressional waves, a fast and a slow wave. These two waves have been identified for the poroelastic case as presented by Schanz and Cheng [9]. To clearly observe these two waves, a semi-infinite column is used to eliminate reflections at the ends that can confuse the arrival of the two different waves. An observation of pressure is made at 5 m below the top surface, where a step stress loading is applied.

Our experience in the poroelastic cases ([9]) has indicated that the second compressional wave dissipates rapidly. With the permeability of these used materials, the second wave will not survive with a detectable magnitude at 5 m below surface. To en-

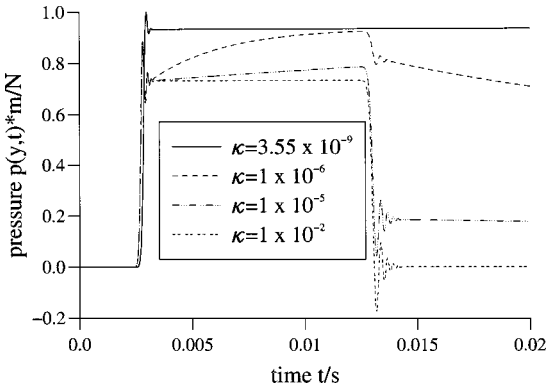

Fig. 5 Pressure $p(t, y=995\,\mathrm{m})$ versus time: wave propagation for different values of κ in an "infinite" soil column

hance the observation of the second wave, artificially large permeabilities, or different materials, must be used. For the present purpose, the permeabilities are arbitrarily increased.

In Fig. 5 the pressure at 5 m below surface in an infinitely long soil column, modeled by $l=1000$ m, caused by a stress Heaviside boundary condition, is plotted versus time for different values of the permeability κ, ranging from 10^{-9} to $10^{-2}\,\mathrm{m}^4/(N\,s)$, and $p_k = p_g = p_{ks} = 1.5(1/s)$. Other material properties are referred to Table 1.

Let us first examine the case with highest permeability, $\kappa = 10^{-2}\,\mathrm{m}^4/(N\,s)$. We observe a step rise in pressure that indicates the arrival of the first wave around 2.5 ms. The pressure stays roughly constant until at 13 ms. At that time, the second wave arrives and negates the positive pressure. Since there is no boundary reflection, the identity of the second wave is clearly established. We should point out that the small fluctuation around the pressure front is an artifact of the numerical method, which generally cannot be avoided. It is, however, small enough to be tolerated. With decreasing permeability, the first wave arrives at increasingly larger amplitude, and the second wave at smaller amplitude. In the case of $\kappa = 3.55\times10^{-9}\,\mathrm{m}^4/(N\,s)$, the curve is flat after the arrival of the first wave, which means that the second wave arrives with an undetectable amplitude due to viscous damping. These dynamic behaviors are similar to those in the poroelastic cases without viscoelasticity, as discussed in more detail in [9].

Once the general dynamic behavior is established, the influence of viscoelasticity in the individual modulus is studied in Fig. 6. As in Fig. 5, the pressure $p(t, y=995\,\mathrm{m})$ due to a stress Heaviside step loading is plotted versus time. But here the cases 1 to 4 defined in the beginning of this section are examined. To enhance the observation of the second wave, the largest permeability case used in the preceding example, $\kappa = 10^{-2}\,\mathrm{m}^4/(N\,s)$, is used here. Similar to the investigation above, the viscoelasticity of different modulus has different effects on the two materials. First of all, we observe that the wave velocities are modified, much more so for the second wave than for the first wave. The arrivals of the first waves are close to each other. Nevertheless, in both materials case 4 gives the slowest first wave. In rock, case 2 has the fastest first wave, and in soil, it is case 3. These are consistent with earlier observations. The second wave, on the other hand, is more complicated. In most cases the second wave of the viscoelastic cases travels faster than the nonviscoelastic one, case 4. However, in case 3, where only the solid grain modulus is modeled viscoelastic, the first wave becomes faster, but the second wave becomes slower than case 4. We also observe that there is significant amplitude reduction of the first wave for the rock material when viscoelasticity is present, except for case 3, where the amplitude increases. For the soil, there is little change in amplitude.

5 Conclusions

In the presented work, Biot's theory of porous media is extended to poroviscoelasticity by means of the elastic-viscoelastic

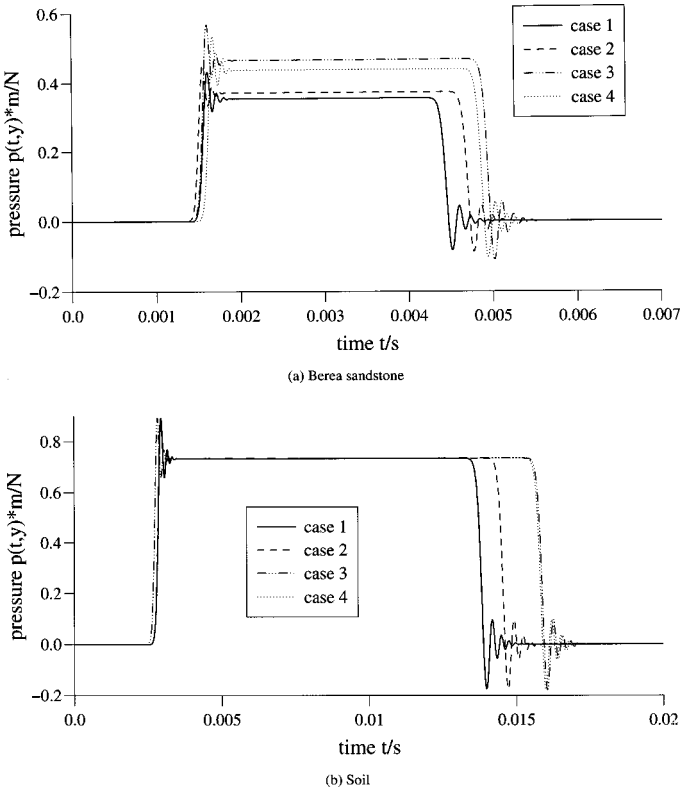

Fig. 6 Pressure $p(t, y=995\,\mathrm{m})$ versus time: wave propagation for different damping cases

correspondence principle. A physically more appealing model is implemented that separates the viscoelasticity to three components—that due to the compression of solid frame, of solid grain, and the shearing of solid frame. A three-parameter rheological model is applied to each of them. The fluid is modeled as viscous and Newtonian, as in the classical theory. Next, an analytical solution of a one-dimensional column is derived in Laplace domain. Then, with the Convolution Quadrature Method the time-dependent behavior is achieved.

Three widely different materials, a rock, a soil, and a sediment, are used in the analysis. The viscoelastic effect is found to be stronger in rock and soil, than in sediment. The rock is shown to be more influenced by the shear modulus whilst the soil is more affected by the compression modulus of the grains. In the frequency domain, shifting of resonance frequencies and damping of resonance peaks are observed. In the time domain with a step stress loading, viscoelastic effect generally leads to an increase in wave speed for both the fast and the slow waves, and a decrease in amplitude, except for case 3 in rock. This shows the conclusions drawn here are not entirely general, and are material dependent.

Acknowledgment

Martin Schanz was supported by the German Research Foundation (DFG) under grant SCHA 527/4-1. The financial support is gratefully acknowledged.

Appendix A

Convolution Quadrature Method. The ''Convolution Quadrature Method'' developed by Lubich numerically approximates a convolution integral

$$y(t)=\int_0^t f(t-\tau)g(\tau)d\tau \rightarrow y(n\Delta t)=\sum_{k=0}^{n}\omega_{n-k}(\Delta t)g(k\Delta t),$$
$$n=0,1,\ldots,N, \tag{31}$$

by a quadrature rule whose weights are determined by the Laplace transformed function $\hat{f}$ and a linear multistep method. This method was originally published in [10] and [19]. Application to the boundary element method may be found in [20]. Here, a brief overview of the method is given.

In formula (31) the time t is divided in N equal steps Δt. The weights $\omega_n(\Delta t)$ are the coefficients of the power series

$$\hat{f}\left(\frac{\gamma(z)}{\Delta t}\right)=\sum_{n=0}^{\infty}\omega_n(\Delta t)z^n, \tag{32}$$

with the complex variable z. The coefficients of a power series are usually calculated with Cauchy's integral formula. After a polar coordinate transformation, this integral is approximated by a trapezoidal rule with L equal steps $2\pi/L$. This leads to

$$\omega_n(\Delta t)=\frac{1}{2\pi i}\int_{|z|=\mathcal{R}}\hat{f}\left(\frac{\gamma(z)}{\Delta t}\right)z^{-n-1}dz$$
$$\approx\frac{\mathcal{R}^{-n}}{L}\sum_{l=0}^{L-1}\hat{f}\left(\frac{\gamma(\mathcal{R}e^{il\,2\pi/L})}{\Delta t}\right)e^{-inl\,2\pi/L}, \tag{33}$$

where $\mathcal{R}$ is the radius of a circle in the domain of analyticity of $\hat{f}(z)$.

The function $\gamma(z)$ is the quotient of the characteristic polynomials of the underlying multistep method, e.g., for a BDF 2, $\gamma(z)=3/2-2z+(1/2)z^2$. The used linear multistep method must be $A(\alpha)$-stable and stable at infinity ([19]). Experience shows that the BDF 2 is the best choice ([21]). Therefore, t is used in all calculations in this paper.

If one assumes that the values of $\hat{f}(z)$ in (33) are computed with an error bounded by ϵ, then the choice $L=N$ and $\mathcal{R}^N=\sqrt{\epsilon}$ yields an error in ω_n of size $\mathcal{O}(\sqrt{\epsilon})$ ([10]). Several tests conducted by the authors lead to the conclusion that the parameter $\epsilon=10^{-10}$ is the best choice for the kind of functions dealt with in this paper ([13]). The assumption $L=N$ results in N^2 coefficients $\omega_n(\Delta t)$ to be calculated. Due to the exponential function at the end of formula (33) this can be done very fast using the technique of the Fast Fourier Transformation (FFT).

References

[1] Biot, M. A., 1941, ''General Theory of Three-Dimensional Consolidation,'' J. Appl. Phys., **12**, pp. 155–164.
[2] Biot, M. A., 1955, ''Theory of Elasticity and Consolidation for a Porous Anisotropic Solid,'' J. Appl. Phys., **26**, pp. 182–185.
[3] Biot, M. A., 1956, ''Theory of Propagation of Elastic Waves in a Fluid-Saturated Porous Solid. I. Low-Frequency Range, II. Higher Frequency Range,'' J. Acoust. Soc. Am., **28**, No. 2, pp. 168–191.
[4] Detournay, E., and Cheng, A. H.-D., 1993, *Fundamentals of Poroelasticity*, Vol. II (Comprehensive Rock Engineering: Principles, Practice & Projects), Pergamon Press, Tarrytown, NY, Chapter 5, pp. 113–171.
[5] Biot, M. A., 1956, ''Theory of Deformation of a Porous Viscoelastic Anisotropic Solid,'' J. Appl. Phys., **27**, No. 5, pp. 459–467.
[6] Wilson, R. K., and Aifantis, E. C., 1982, ''On the Theory of Consolidation With Double Porosity,'' Int. J. Eng. Sci., **20**, pp. 1009–1035.
[7] Vgenopoulou, I., and Beskos, D. E., 1992, ''Dynamic Behavior of Saturated Poroviscoelastic Media,'' Acta Mech., **95**, pp. 185–195.
[8] Abousleiman, Y., Cheng, A. H.-D., Jiang, C., and Roegiers, J.-C., 1996, ''Poroviscoelastic Analysis of Borehole and Cylinder Problems,'' Acta Mech., **109**, No. 1–4, pp. 199–219.
[9] Schanz, M., and Cheng, A. H.-D., 2000, ''Transient Wave Propagation in a One-Dimensional Poroelastic Column,'' Acta Mech., **145**, No. 1-4, pp. 1–8.
[10] Lubich, C., 1988, ''Convolution Quadrature and Discretized Operational Calculus. I.,'' Numer. Math., **52**, pp. 129–145.
[11] Narayanan, G. V., and Beskos, D. E., 1982, ''Numerical Operational Methods for Time-Dependent Linear Problems,'' Int. J. Numer. Methods Eng., **18**, pp. 1829–1854.
[12] Cheng, A. H.-D., Sidauruk, P., and Abousleiman, Y., 1994, ''Approximate Inversion of the Laplace Transform,'' Mathematica J. **4**, No. 2, pp. 76–82.
[13] Schanz, M., and Antes, H., 1997, ''Application of 'Operational Quadrature Methods' in Time Domain Boundary Element Methods,'' Meccanica, **32**, No. 3, pp. 179–186.
[14] Christensen, R. M., 1971, *Theory of Viscoelasticity*, Academic Press, New York.
[15] Bonnet, G., and Auriault, J.-L., 1985, ''Dynamics of Saturated and Deformable Porous Media: Homogenization Theory and Determination of the Solid-Liquid Coupling Coefficients,'' N. Boccara and M. Daoud, eds., *Physics of Finely Divided Matter*, Springer-Verlag, Berlin, pp. 306–316.
[16] Cheng, A. H.-D., Badmus, T., and Beskos, D. E., 1991, ''Integral Equations for Dynamic Poroelasticity in Frequency Domain With BEM Solution,'' J. Eng. Mech. **117**, No. 5, pp. 1136–1157.
[17] Kim, Y. K., and Kingsbury, H. B., 1979, ''Dynamic Characterization of Poroelastic Materials,'' Exp. Mech., **19**, pp. 252–258.
[18] Badiey, M., Cheng, A. H.-D., and Mu, Y., 1998, ''From Geology to Geoacoustics—Evaluation of Biot-Stoll Sound Speed and Attenuation for Shallow Water Acoustics,'' J. Acoust. Soc. Am., **103**, No. 1, pp. 309–320.
[19] Lubich, C., 1988, ''Convolution Quadrature and Discretized Operational Calculus. II,'' Numer. Math., **52**, pp. 413–425.
[20] Schanz, M., and Antes, H., 1997, ''A New Visco- and Elastodynamic Time Domain Boundary Element Formulation,'' Comput. Mech., **20**, No. 5, pp. 452–459.
[21] Schanz, M., 1999, ''A Boundary Element Formulation in Time Domain for Viscoelastic Solids,'' Commun. Numer. Meth. Eng. **15**, pp. 799–809.